

Validation of a Thermal Radiation Problem using *BOUNDARY_RADIATION_ENCLOSURE

Gunther Blankenhorn¹, Bobby Gyesei², Skye Malcolm², Imtiaz Gandikota¹, Roger Grimes¹, Francois-Henry Rouet¹

¹Livermore Software Technology Cooperation (LSTC)

²Honda R&D Americas, Inc.

1 Introduction

Thermal radiation problems are gaining interest in the automotive industry. Examples include paint drying and curing processes, determining material characteristics and deformation due to heat treatment, temperature distributions in muffler systems and heat shields in engine compartments.

LS-DYNA has capabilities to couple the thermal solver with mechanical and multi physics solver. Solving for thermal convection, conduction and contact in three dimensions are already available in all parallel models LSTC are offering, namely shared memory parallel (SMP), massive parallel processor (MPP) and the combination of both models (HYBRID). Lately the thermal radiation feature has been extended to be used with massive parallel processor (MPP) version and a new solver to solve for radiosity.

New developments are tested with verification examples and small test cases to determine the code functionality and expected results. Furthermore they have to show their applicability with validations of numerical models with experimental data. They also need to be evaluated regarding their scalability of wall clock time to reduce costs of compute resources.

This contribution addresses two of these subjects, the scalability and the validation.

The validation example used here is a part of a B-pillar which is heated up in an oven. Temperatures were measured at several locations of the sheet metal. Test data was provided by Honda R&D Americas, Inc.

The test was modeled as a thermal radiation problem in an enclosure. Thermal radiation was modeled using the keyword ***BOUNDARY_RADIATION_ENCLOSURE** and was performed in LS-DYNA MPP. An LS-DYNA MPP scalability study was performed. Due to missing data for the thermal parameters, the heat capacity, thermal conductivity and emissivity were determined with LS-OPT.

2 Implementation

Thermal radiation is the heat transfer between two surfaces via electromagnetic radiation. In LS-DYNA, these surfaces are created by segments on the free faces of the element. These segments are used to define view factors (see [1] and [2]) which are later used to solve for radiosity. A view factor can be defined as:

$$F_{1 \rightarrow 2} = \frac{1}{A_1} \int_{A_1} \int_{A_2} \frac{\cos \theta_1 \cos \theta_2}{\pi s^2} dA_2 dA_1 \quad (1)$$

where $F_{1 \rightarrow 2}$ describes the proportion of thermal radiation which leaves surface 1 and reaches surface 2. θ_1 and θ_2 are defined as angles between the surface normal and the sightline of the surface midpoints, s is the length of the sight line and A_1 and A_2 are the surface areas of surface 1 and surface 2. The view factors can be ordered in a matrix form, which is used to solve for radiosity:

$$\left[\delta_{ij} - \frac{(1-\varepsilon_i)}{A_i \varepsilon_i} F_{ij} \right] \cdot B_i = \sigma T_i^4 \quad (2)$$

where δ_{ij} is the Kronecker delta, ε_i is the emissivity of segment i , A_i is the surface area of segment i , F_{ij} is the view factor matrix, σ is the Stefan-Boltzmann constant, T_i are the temperature of segment i and B_i is the radiosity of segment i . These equations are solved using a Conjugated Gradient method.

The radiation problem needs a reasonably fine mesh to produce accurate results. Ideally, meshes from structural models should be reused for the thermal or later for a coupled thermal structural calculation.

The number of view factors increase with $O(N^2)$ with N being the number of segments in the radiation enclosure problem. This is challenging for memory requirements and computation time. Therefore LS-DYNA used to offer a feature to calculate view factors in the MPP version. These view factors would be written to an ASCII file, which could be read by the LS-DYNA SMP version to solve the radiation problem.

Starting with LS-DYNA R12, this feature has been extended to calculate the view factors and solve the radiation problem in on run with LS-DYNA MPP. These efforts are mainly driven by higher segments counts and the need to couple the thermal radiation feature with LS-DYNA fluid solvers for calculations which cannot be done efficient with the SMP version of LS-DYNA.

The MPP feature will undergo continuous improvements to meet future requirements. One key requirement is to reduce wall clock time, the time the calculation needs to finish the analysis. This time measure should be decrease with increasing number of ranks for the MPP parallel model. A study was carried out to determine the speed up of the calculation. Result can be found in section 5.

3 Experimental set up and results

The physical test was performed at Honda R&D Americas, Inc. Ohio. A part was cut out of the B-pillar (see Fig. 1) and heated up in a small oven. Initial oven temperature was 200° Celsius. Two groups of thermal sensors, "MP_pair" group and "MP_sheet" group, were placed on the sheet metal (see Fig. 3 and Fig. 5) and time series of temperature was recorded for these sensors (see Fig. 2 and Fig. 4). The locations of these sensors are marked with a green dot in Fig. 3 and Fig. 5. The experiment lasted 1 hour. At the end of the experiment the B-pillar part had a temperature close to the oven wall temperature, which was assume to be 200° Celsius.

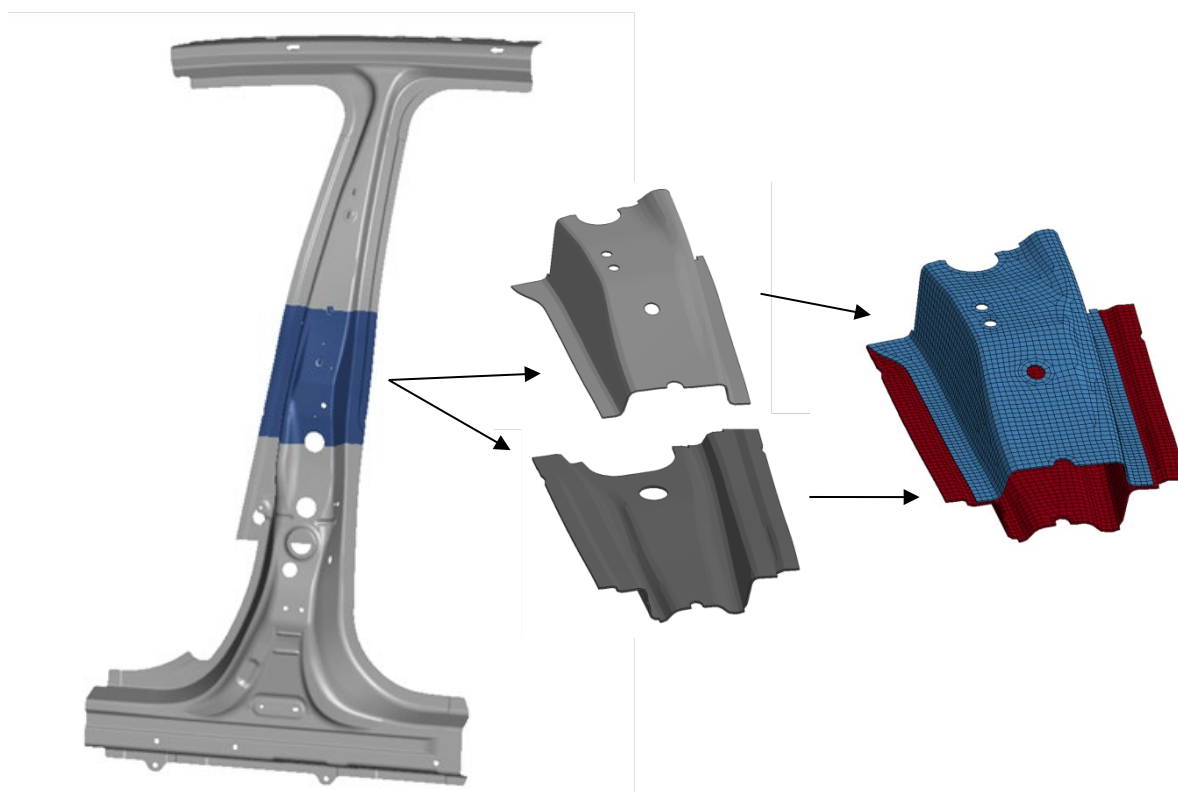


Fig. 1: B-pillar part location (blue), geometry and finite element mesh (thick shell).

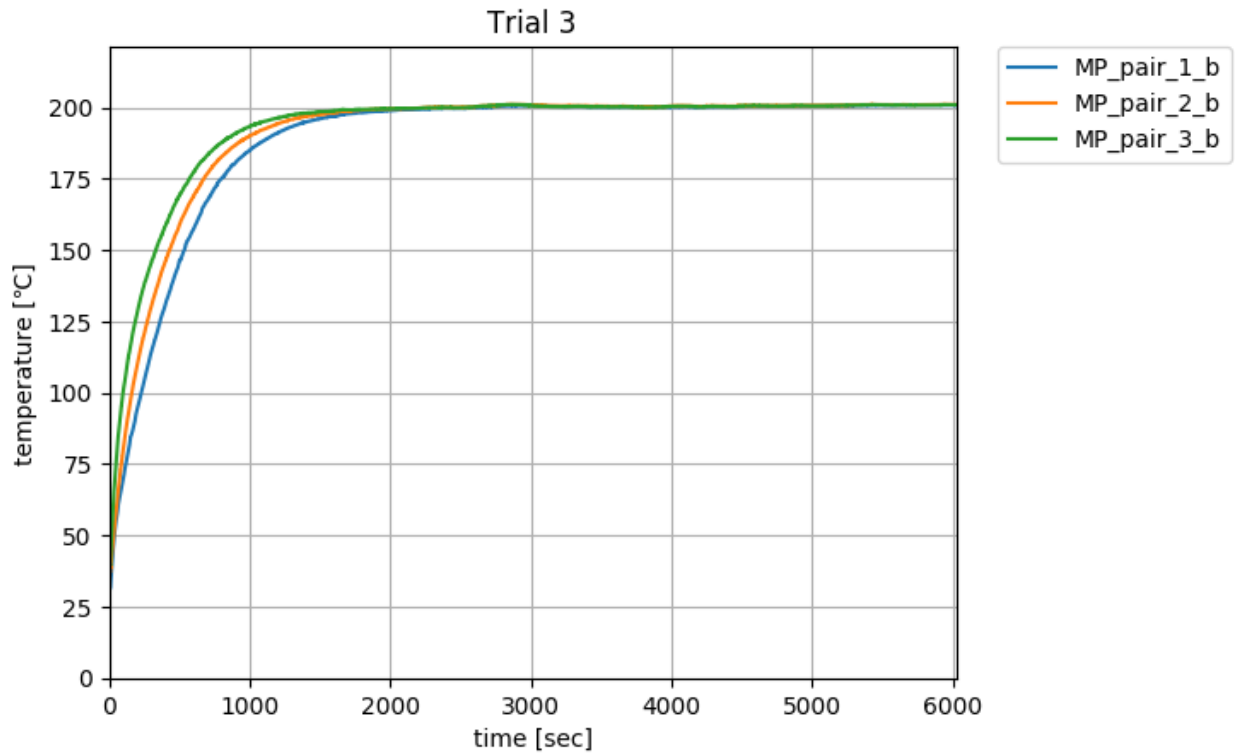


Fig. 2: Experimental results for the “MP_pair” group of temperature sensors (Trial 3)

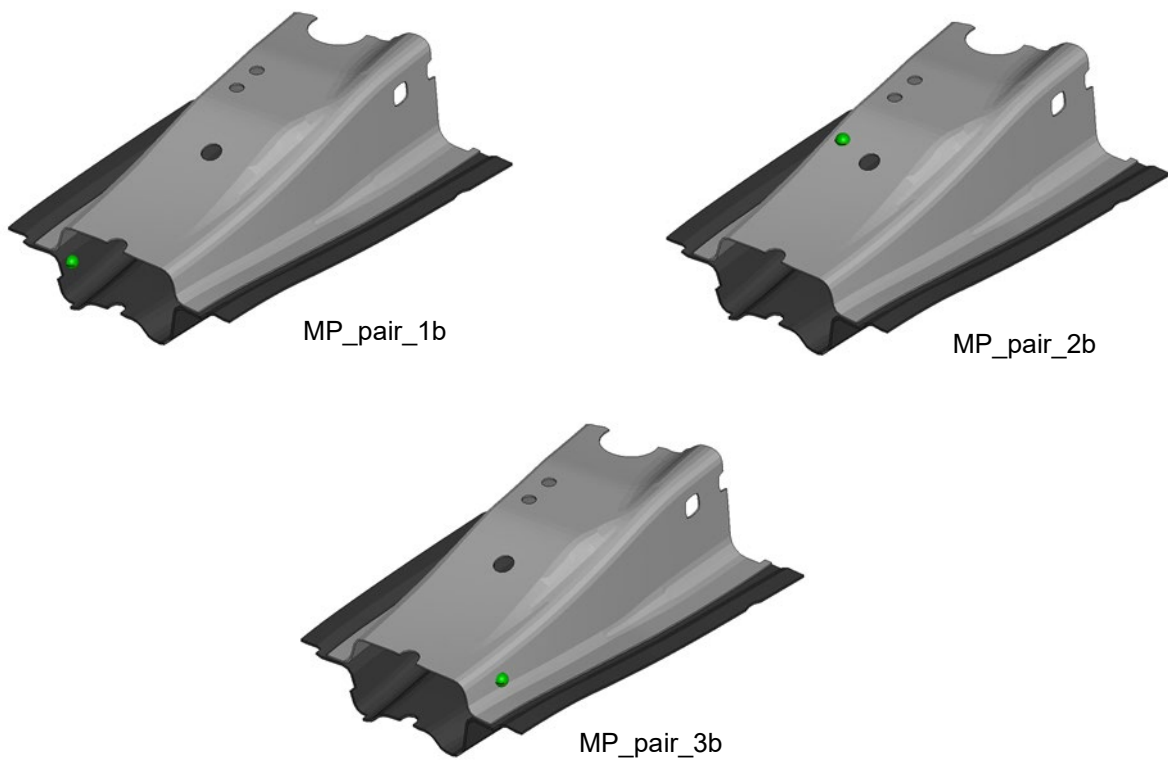


Fig. 3: Sensor location (green dot) of “MP_pair” group of temperature sensors

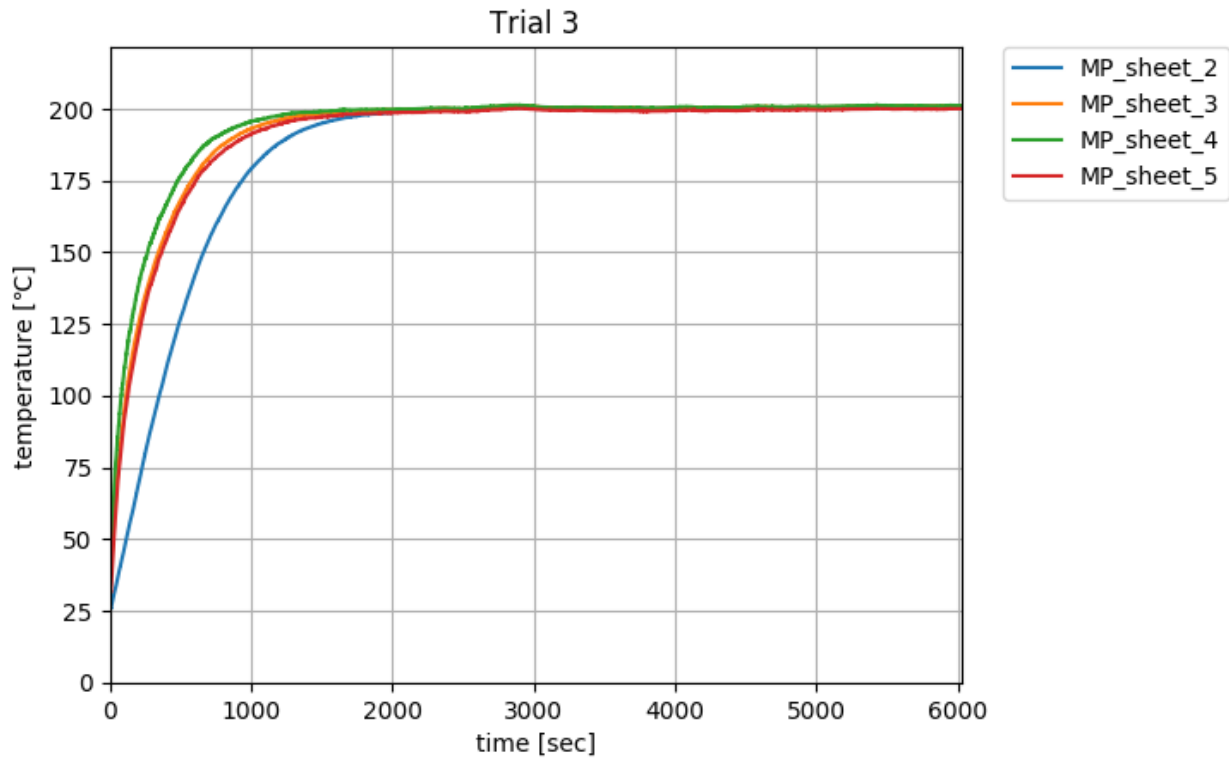


Fig. 4: Experimental results for the “MP_sheet” group of temperature sensors (Trial 3)

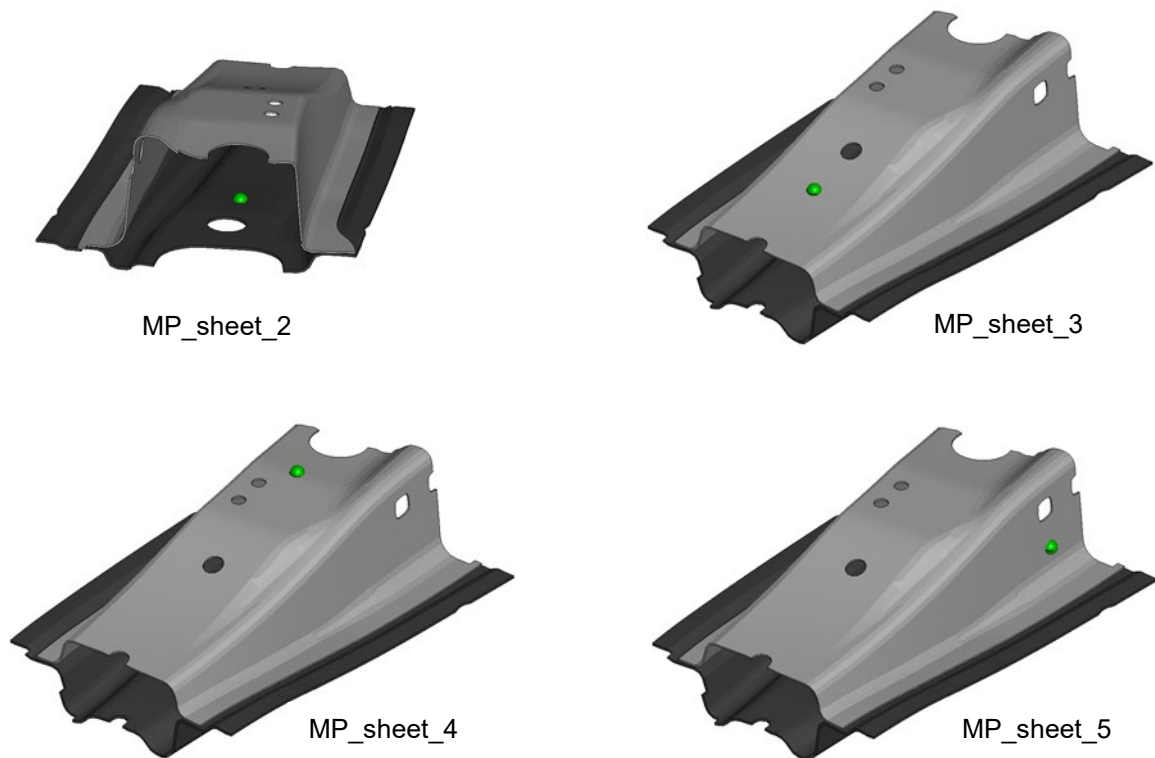


Fig. 5: Sensor location (green dot) of “MP_sheet” group of temperature sensors

4 Finite element model

The B-Pillar part was modeled with thick shell elements and the oven structure was modeled with solid elements. Segments are defined on the free surfaces of the tick shells and the inside of the oven. These segments were included in the thermal radiation enclosure. Element, nodes and segment counts can be found in Table 1.

item	count
Solids (oven)	728
Thick shells (B-pillar part)	5142
nodes	12154
Thermal radiation segments	10715

Table 1: Finite element model counts

The model and results of a test run are displayed in Fig. 1. Parameters for heat capacity, thermal conductivity, and emissivity of both B-pillar and oven were not available and determined via a parameter identification using LS-OPT (see section 6).

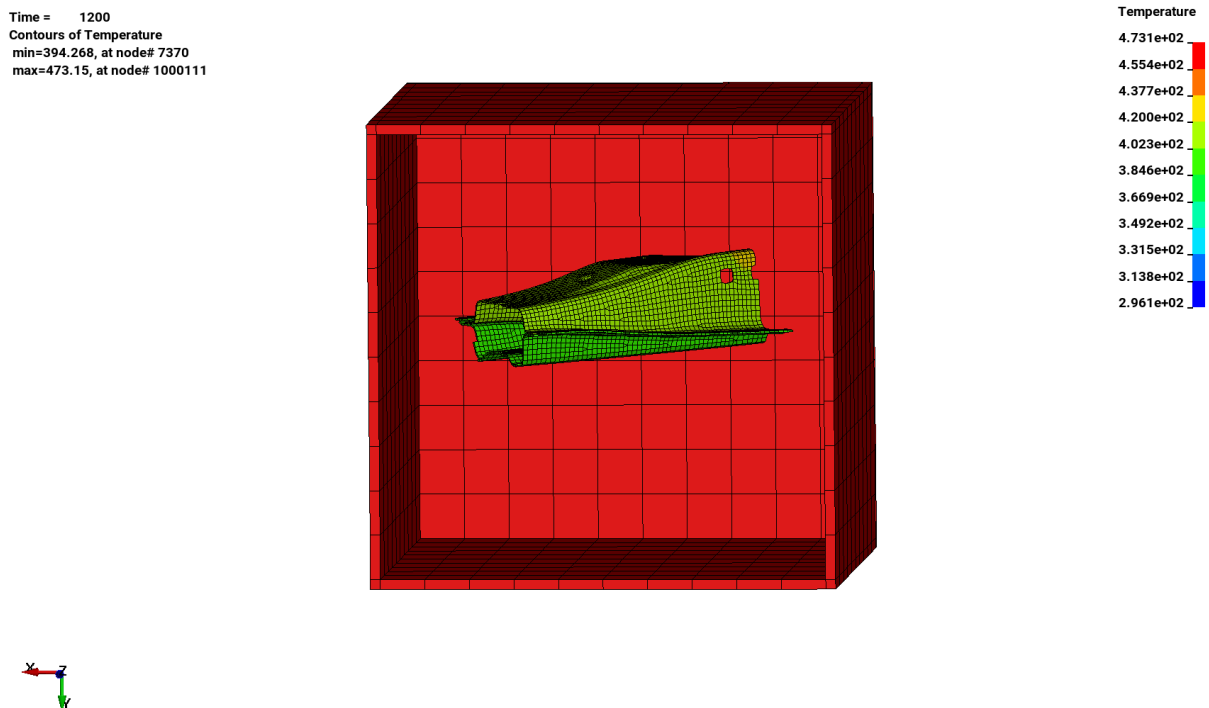


Fig. 6 Temperature plot, 1200 seconds in the experiment, oven wall temperature at 200 Celsius, b-pillar part is heating up.

5 Scalability

Scalability is defined here as the ability to reduce wall clock time if more MPP ranks are added to the execution of LS-DYNA MPP. The input and the environment are kept unchanged for this study.

A total of 8 runs were performed here to determine scalability. MPP rank counts included 1, 2, 4, 12, 24, 48, 96, and 192 MPP ranks. Specification of the used hardware can be found in Table 2. Results are presented in the measure of “speed up”. “Speed up” is defined here as the relation of wall clock time of one rank to the wall clock time of several ranks. Results of this study are displayed in Fig. 7. A speed up is achieved with higher rank counts, but the speed up is lower as the ideal speed up. Investigation to improve the scalability are a currently under investigation.

item	count
CPU type	Intel® Xeon® E5520 (2.27GHz)
Interconnect	InfiniBand
cores per node	8

Table 2: Finite element model counts

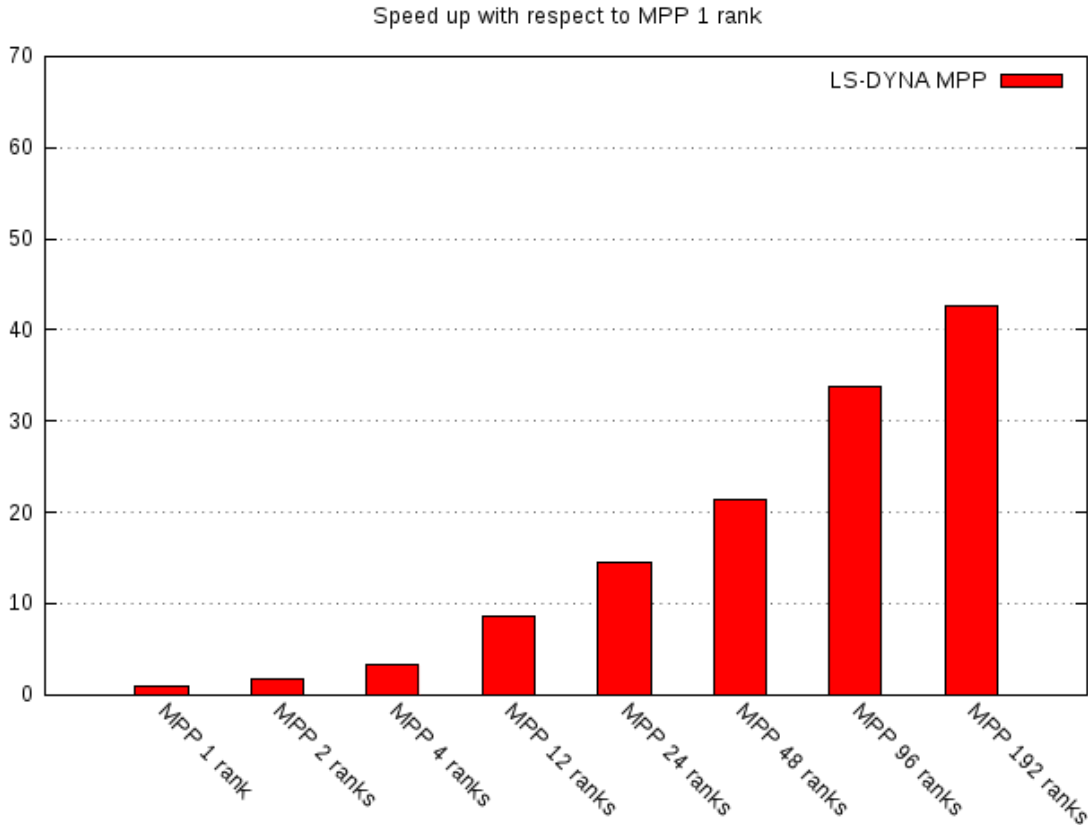


Fig. 7: Speed up for different MPP rank counts.

6 Parameter identification

6.1 Setup

LS-OPT design optimization tool was used to identify the unknown thermal parameters. A total of 6 parameters, heat capacity, thermal conductivity, and emissivity of both b-pillar and oven, were selected for optimization. The design variables and their respective lower and upper bounds are shown in Table 3 and Table 4 below. The temperature of “pair” and “sheet” group of sensors, extracted from LS-DYNA, were matched with the experimental data using mean square error method. Therefore, the goal of the optimization is to minimize the total mean squared error between points of seven pairs of simulation and experimental data. To save computation cost and quickly converge to a solution, metamodel-based sequential optimization with domain reduction was selected as optimization strategy in LS-OPT. The optimization problem can be formulated as,

$$\min \sum_{l=1}^L \sum_{p=1}^P \frac{1}{P} (f_p(x) - F_p)^2 \quad (3)$$

where, L represent the number of curves being matched, x are the design variables, P are the number of regression points for each curve, and f, F represent the metamodel predicted value and experimental data at point p , respectively. Since temperature histories are not yet supported in LS-OPT, a postprocessing stage was include in the setup and GenEx tool was used to extract temperature histories from “tprint” ASCII file. The optimization setup in LS-OPT is shown in Fig. 8.

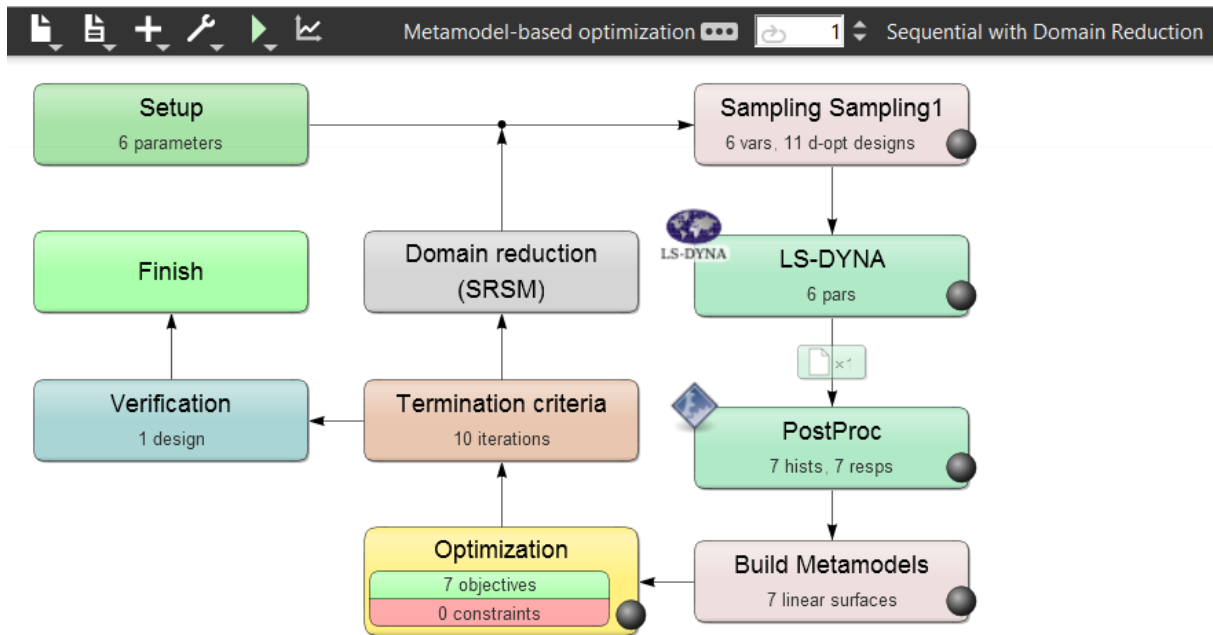


Fig. 8: LS-OPT optimization setup

Parameter	Lower Bound	Upper Bound
Emissivity	0.2	0.7
Heat capacity	4.6 E+08	5.1 E+08
Thermal conductivity	12.0	54.0

Table 3: Parameter intervals assigned to B-pillar part.

Parameter	Lower Bound	Upper Bound
Emissivity	0.07	0.5
Heat capacity	4.6 E+08	5.1 E+08
Thermal conductivity	12	54

Table 4: Parameter intervals assigned to oven.

6.2 Results parameter identification

The optimal parameter set obtained by the LS-OPT parameter identification can be found in Table 5.

Parameter	B-pillar part	Oven
Emissivity	0.79909033	0.553880704
Heat capacity	4.80995200 E+08	4.85269935 E+08
Thermal conductivity	12.00	51.9834853

Table 5: Optimal Parameters assigned to B-pillar part and oven.

Optimization history for sensor location MP_pair_1b is displayed in Fig. 9. The temperature time series are color coded with respect to the iterations of the LS-OPT optimization. The dark blue temperature curve represents the first iteration and the red temperature curve the results obtained with the parameter set listed in Table 5. The black curve represents the temperature time data from the sensor obtained by the experiment.

Fig. 10 to Fig. 16 display the results obtained with the parameter set listed in Table 5 for sensor location of the “MPP_pair” and “MP_sheet” group. Here the color of the temperature time series

corresponds with the emissivity range on the right side of the plot. The black curve represents the temperature time data from the sensor obtained by the experiment.

Results are close to the experimental data. The time series for sensor location MP_pair_1b and MP_sheet_2 are not as close to experimental data as the temperature time series of the other sensor locations.

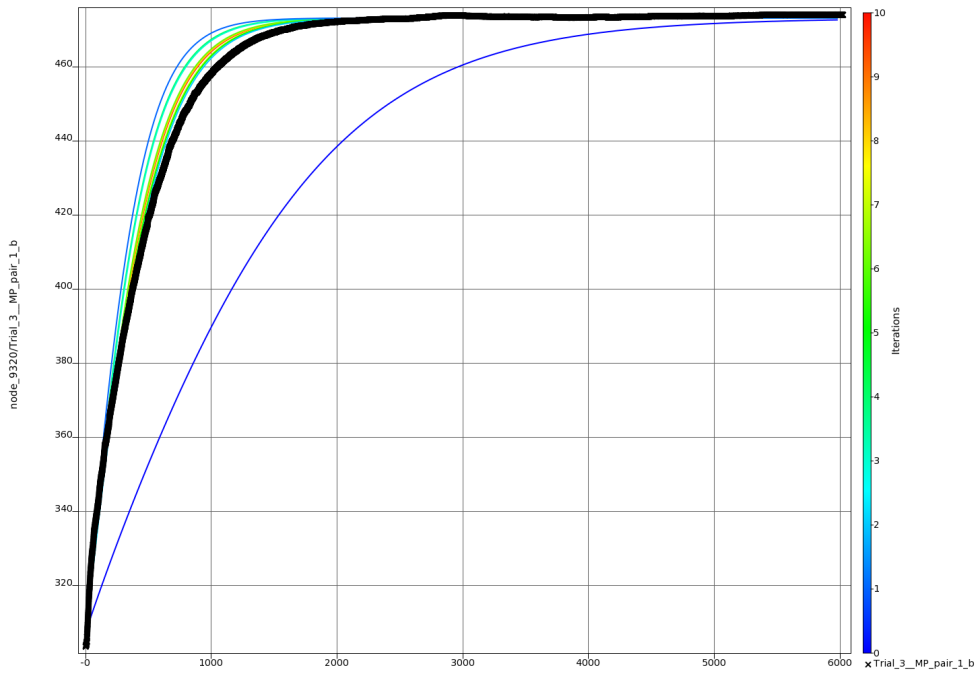


Fig. 9: Optimization history: temperature on sensor MP_pair1b location

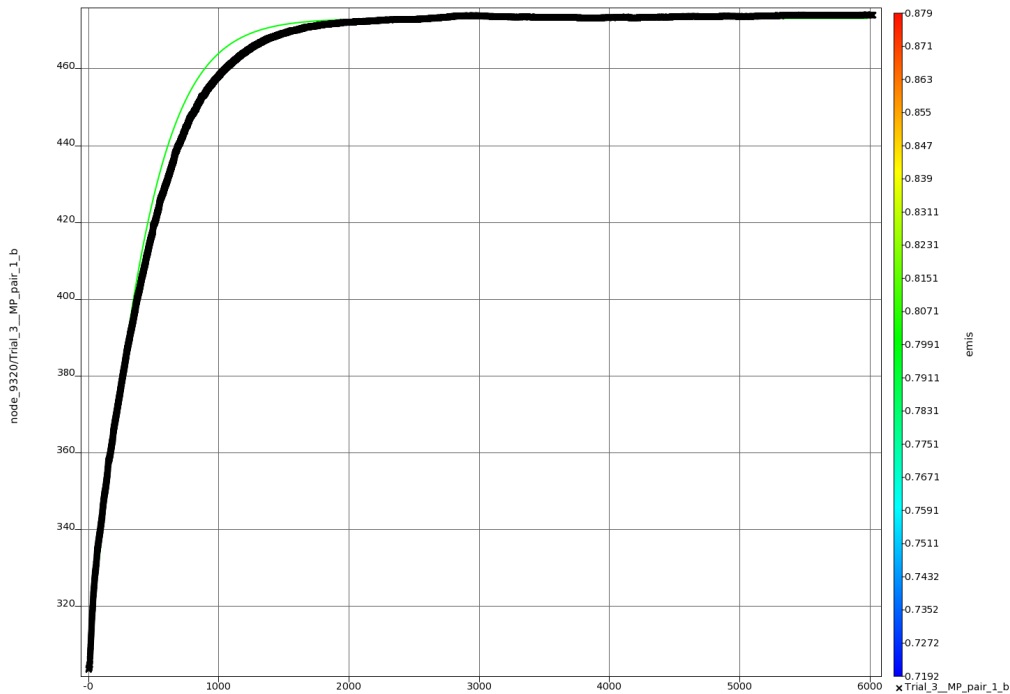


Fig. 10: Temperature time series for optimal parameter set – sensor location MP_pair_1b

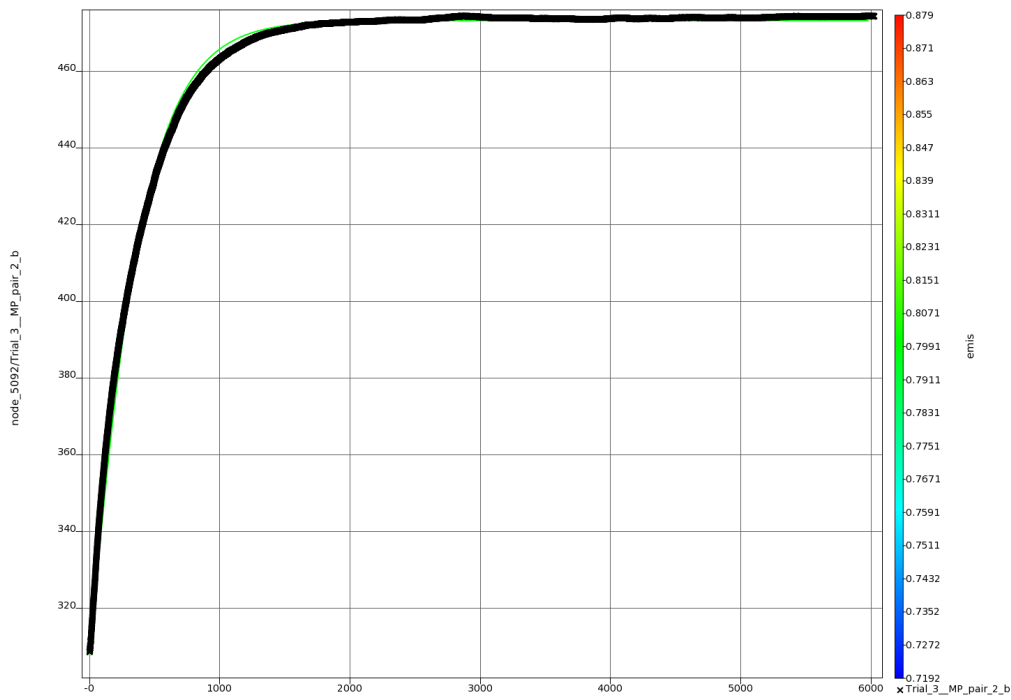


Fig. 11: Temperature time series for optimal parameter set – sensor location MP_pair_2b

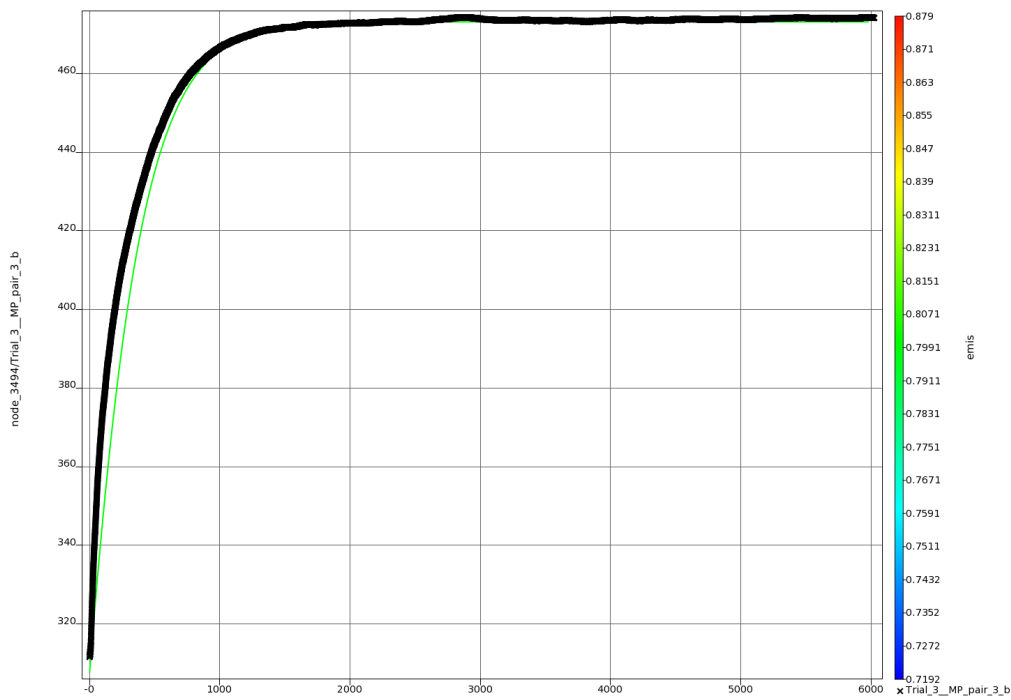


Fig. 12: Temperature time series for optimal parameter set – sensor location MP_pair_3b

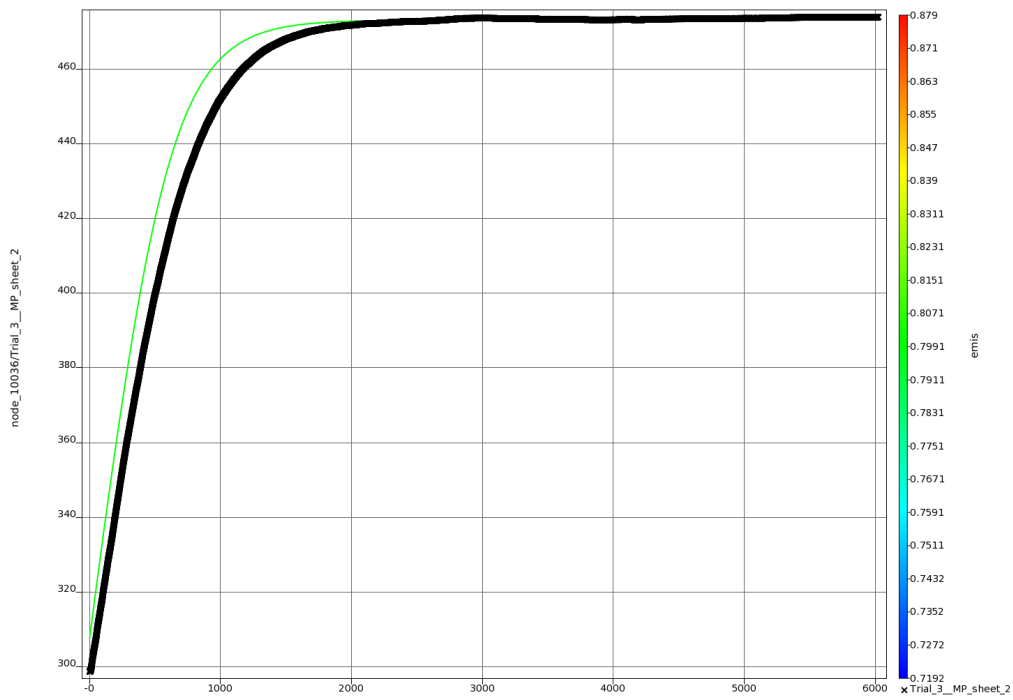


Fig. 13: Temperature time series for optimal parameter set – sensor location MP_sheet_2

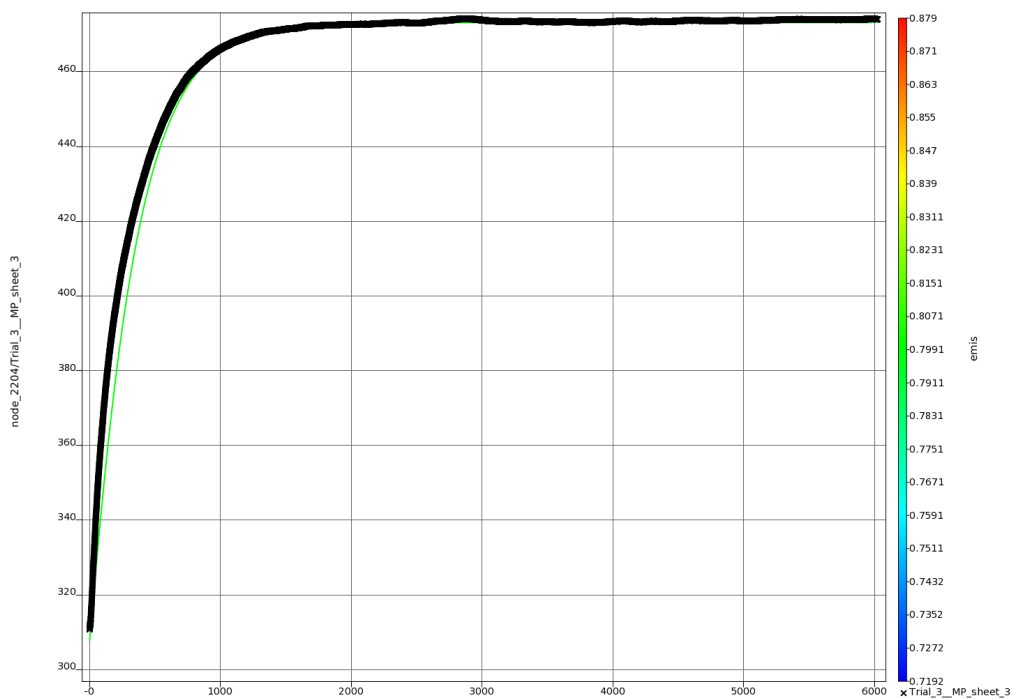


Fig. 14: Temperature time series for optimal parameter set – sensor location MP_sheet_3

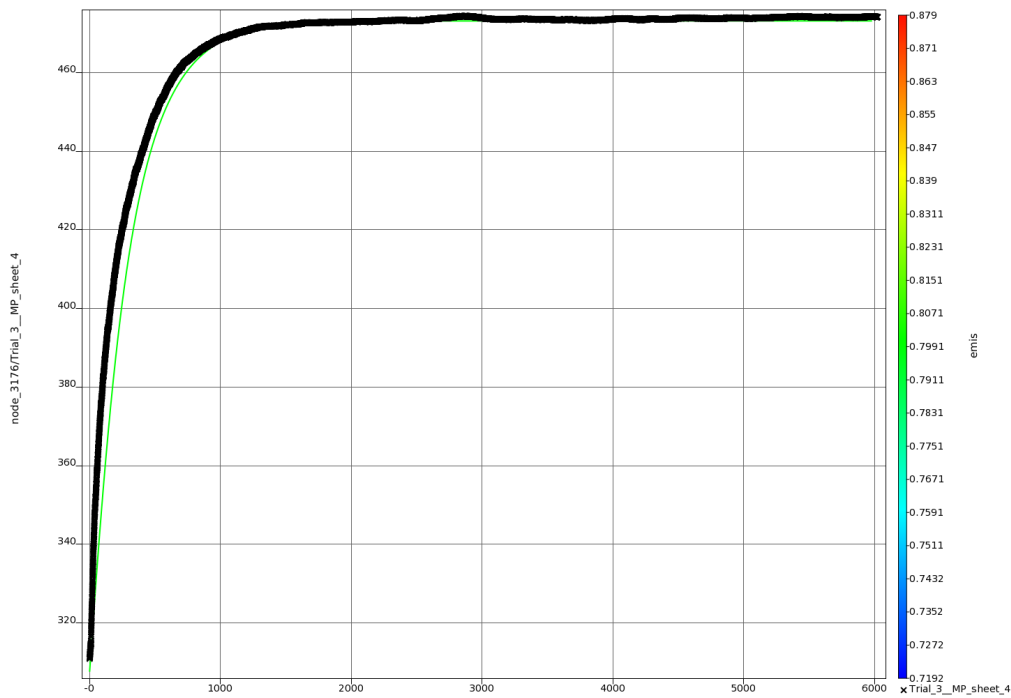


Fig. 15: Temperature time series for optimal parameter set – sensor location MP_sheet_4

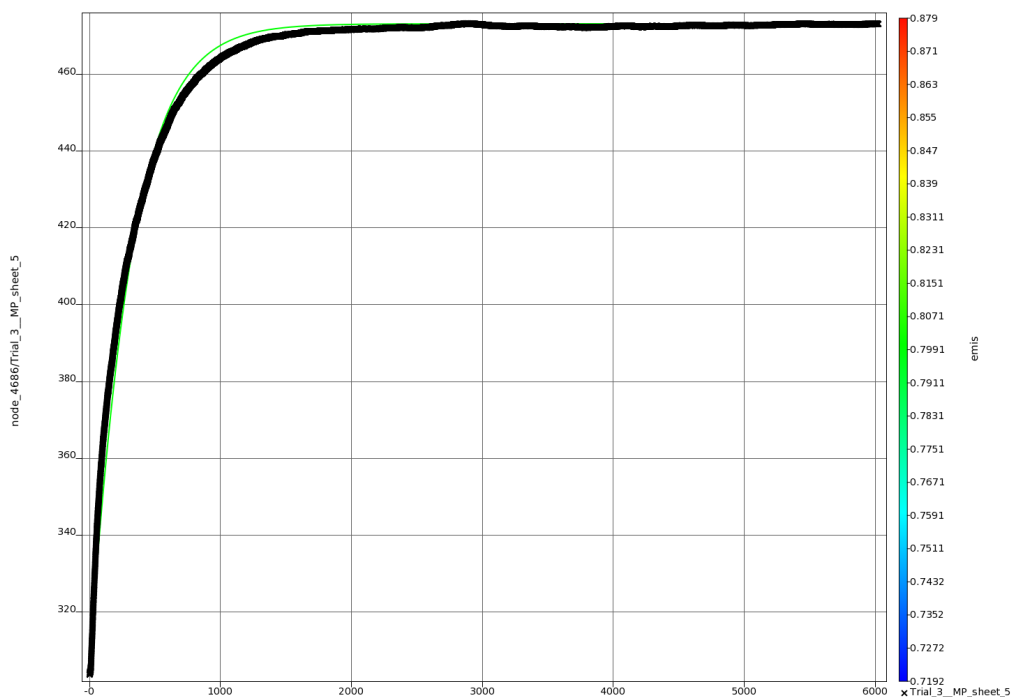


Fig. 16: Temperature time series for optimal parameter set – sensor location MP_sheet_5

7 Summary

The validation study of a B-pillar part in an oven was carried out using the keyword ***BOUNDARY_RADIATION_ENCLOSURE**. LS-DYNA MPP was used throughout the study. Results were compared to experimental data provided by Honda R&D Americas, Inc.

MPP Scalability was determined for this problem. Speedup can be shown. The decrease of speed up with higher ranks counts may show room for improvement on the scalability side of the current implementation.

Thermal material parameters were unknown for the experiment and were determined by a parameter identification performed with LS-OPT.

Validation Results are promising for modeling the effects of thermal radiation with this keyword. It is worth mentioning that the results of two of the seven sensor locations show a bigger discrepancy than the other five. These two sensor locations are on the inside of the B-pillar part. This may need further investigation.

8 Acknowledgements

The authors wish to thank Honda R&D Americas, Inc. for supporting this validation effort and providing experimental data and geometry data for this study.

9 Literature

- [1] Shapiro, A, FACET – A Radiation View Factor Computer Code for Axisymmetric, 2D Planar, and 3D Geometries with Shadowing, August 1983, Lawrence Livermore Laboratory
- [2] Sparrow, E.M. and Cess, R.D., Radiation heat transfer, 1966, Brooks Pub. Co.